Classification and localization of gastric cancer using Multi-Information Fusion Network

Varghese Sicily Felix ENIGO*, Rajashree SHANMUGANATHAN, Sneha VENKATAPATHY, Sahir RAHAMAN

Department of Computer Science & Engineering,
Sri Sivasubramaniya Nadar College of Engineering, Chennai, Tamil Nadu, India

felixvs@ssn.edu.in*****, rajashree18122@cse.ssn.edu.in, sneha18701@cse.ssn.edu.in, sahir18129@cse.ssn.edu.in

***Corresponding author:** Varghese Sicily Felix ENIGO
felixvs@ssn.edu.in

Abstract: Diagnosing and differentiating gastric cancer cells from stomach ulcers requires high-domain expertise and is time-consuming. Furthermore, medical image processing requires extremely high segmentation accuracy, which may lack interpretability and therefore, cannot be trusted by professional doctors for clinical application Hence, a diagnosis support system is proposed to aid pathologists and gastroenterologists that employs a deep learning network known as Multi-Information Fusion Network (MIFNET) for detecting cancer cells from histopathological images. The proposed system will offer assistance to gastroenterologists by displaying the severity level of the cancer, thereby helping them in choosing the appropriate treatment to increase the patient survival rates for those with stomach cancer. In contrast to conventional MIFNET segmentation functionality, the Fusion net layer of MIFNET was modified with VGG16 for classifying the malignant lesions in the gastric lining. The proposed MIFNET-based model results in a segmentation accuracy of 83% and a classification accuracy of 99%. Moreover, it is proven that the model achieved better prediction accuracy than other deep learning models such as U-Net and V-Net.

Keywords: Gastric Cancer, Mifnet, Deep Learning, Image Segmentation, U-Net, V-Net, Classification, Histopathological Images.

1. Introduction

Cancer is defined as the abnormal proliferation of cells in any organ of the body. In essence, the cells in those organs have hit their development limit. These silent and saturated cells reproduce fast until they are either removed physically through surgery, medicine, hormone therapy, or radiation therapy, or they naturally dissipate. The epithelial cells that line the stomach are where gastric cancer (GC) typically arises. According to data from throughout the world, stomach cancer is the second most prevalent cancer and the fourth most common cancer overall (Katai et al., 2018; Li et al., 2018; Siegel et al., 2023). The impact of various factors, including environment and genetics, on the occurrence and progression of stomach cancer has not been fully explored, and the impact of these factors on the development of gastric cancer has not been fully clarified. Even with intensive therapy that includes surgery, chemotherapy, and radiotherapy, less than 30% of patients with advanced stomach cancer survive for five years (Miller et al., 2016). Early stomach cancer treatment has a five-year survival rate of more than 90%, with some patients even attaining curative results (Bray et al., 2018). Stomach cancer is caused by the proliferation of malignant cells in the stomach lining. This malignancy is also known as stomach cancer, and it is difficult to identify early using tumor markers because most people do not exhibit symptoms. Also, early identification using imaging diagnosis examination (Doyama et al., 2015; Huneburg et al., 2016; Van der Post et al., 2018; Zhang et al., 2022) has some limitations due to the subjective nature and uncertainty of lesions (Duffy et al., 2014). As a result, it typically goes undiagnosed until cancer has spread to other parts of the body.

Deep learning has become the most widely used machine learning for disease diagnosis due to the prevalence of diagnostic imaging in clinical diagnostics and the natural applicability of deep learning algorithms for the recognition of images. Although trained medical professionals effectively detect diseases, decision-making is time-consuming and difficult. DL models can infer important information for diagnosis by directly extracting features in the raw from large datasets to aid in clinical decision-making. Although it is natural to add more layers in deep learning to boost

https://doi.org/10.33436/v33i4y202309

representational capacity, doing so does not effectively reflect the global context and instead makes computing more complex and training more challenging (Li et al., 2019). The attention-guided multi-scale learning network for automatic prostate and tumor segmentation (Li et al., 2023) is performed on MRI not using histopathological images.

On the other hand, MIFNET has demonstrated superior edge detection and image segmentation in images with complex textures and intensity distribution, such as in Sea-Land segmentation (Zhihong et al., 2018). MIFNET uses three components to perform this: a multi-tasking network, a global network, and a fusion network for precise segmentation. In the proposed system, the fusion net was modified with VGG16 layers for disease stage classification. Together, globalnet and multitasknet can identify cancerous cells with ill-defined borders. For network learning, it accomplishes this by analyzing multi-scale edges, multi-scale segmentation data, and global context data.

Because malignant cells lack clearly defined borders, some cells may likely be mistakenly labeled if only local information is taken into account. Since carcinogenic tumors are distinguished by their asymmetrical shape and poor edge developments, identifying irregularities along the gastric lining might provide information about a probable malignant tumor that may cause gastric cancer. Thus, the modified MIFNET provides an end-to-end multi-information fusion paradigm for detecting and classifying gastric cancer.

The proposed MIFNET architecture with the updated fusion net for GC classification is shown in Figure 1. MIFNET helps in timely diagnosis and prognostic evaluations, improving the survival rate of gastric cancer patients. This will help lower the high incidence and mortality of GC.

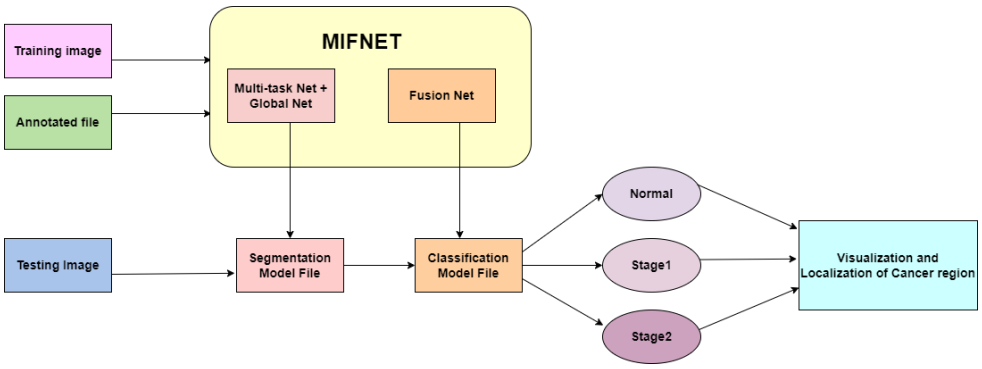

Figure 1. Architecture Diagram of the proposed system

The following briefly summarizes major contributions: To combine local multi-scale edge and segmentation maps with global contextual data from the input images, we use a Multitask Network and GlobalNet.

A modified Fusion Net with VGG16 architecture is presented, that classifies the images as normal, stage-1, or stage-2 cancer based on the segmentation results of Multitask Net and GlobalNet.

Along with the classification results, we create a visualization of the location of the cancer cell to aid clinicians in easily locating the cancerous cells.

2. Methods

The proposed system for localizing and identifying the severity level of gastric cancer includes the following steps: Image Normalization, Image Augmentation, Training, and Testing.

2.1. Preprocessing and augmentation

The histopathological images used in this work are obtained from Seed Gastric Carcinoma Dataset (Wang, 2021). The data is split in the ratio of 70% for the Training set and 30% for the Testing set.

The images are resized to 224*224 making it suitable for the deep learning model, thereby increasing the accuracy and efficiency of the model. The aspect ratios are changed to maintain uniformity within the images. The images are rotated, shifted, and flipped and 2000 images are finally obtained. Data augmentation is performed due to the limitations involving a large dataset of medical images required to train deep-learning models. Due to data privacy laws governing the use of medical images, it is not profitably feasible to procure such large datasets for research purposes. To improve the validation efficiency, medical images are not zoomed or sheared. The dataset was split into the ratio 75:25 where 1500 images were used for training purposes and the remaining 500 images were used in the testing set. The cancer cells in the images are annotated by an expert in the field of gastroenterology using an online tool for labelling data called Makesense.ai. The annotations are stored in a JSON file, which is used later by the deep learning model for training and validation purposes.

2.2. Framework architecture

MIFNET (Multi Information Fusion Network) consists of three networks - MultiTaskNet, GlobalNet, and FusionNet. The network architecture is depicted in Figure 2. The core idea is to integrate multiscale borders multiscale classification, and global factors via network learning. The multitasking network produces multiscale edge maps and multiscale classification outputs. The segmentation produced by a combined global context and local information is generated by the global network. The Fusion network uses the Multitasknet and GlobalNet segmentation results to classify the images as stage 1, stage 2, or normal.

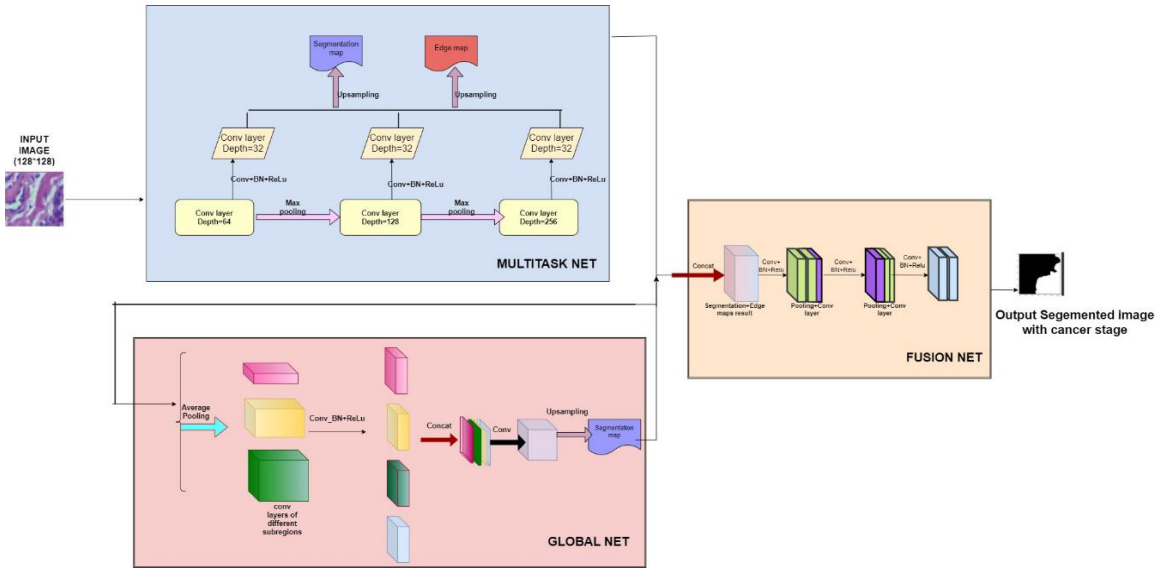

Figure 2. Mifnet Architecture Diagram

2.1.1. Multitask Network

Convolutional and max-pooling layers make up most of the down-sampling path, which is in charge of high-level feature extraction. As shown in Figure 2, the down-sampling path's structure, which consists of four convolution blocks, is comparable to that of VGG (Hirasawa et al., 2018). Each convolution block has two or three convolutional layers with kernel size 33 and stride 1, followed by a max-pooling layer with kernel size 22 and stride 2. Batch normalization (Ishihara et al., 2017) and rectified linear units (Sakai et al., 2018) are performed successively after each convolutional layer. Dilated convolution uses a dilated ratio in the range of 1 to 3 in the last convolution block to increase the receptiveness. The degree of receptiveness is high for a deeper network. The lower-level attributes eventually become higher-level attributes with more semantic data corresponding to different scales of information. The down-sampling approach gets high-level features because of max pooling, but edge details are lost as the spatial resolution rapidly

decreases. This issue can be resolved by using edge information to increase edge precision. As a result, a multi-tasking module in the up-sampling path is constructed that carries out edge detection as well as segmentation of cancer cells. The information about the edges of cancer cells is lost during the down sampling of images, which is crucial for the algorithm to detect cancer cells during training and validation. Depth features are integrated with multitask components using a convolutional layer with feature maps at various scales. The segmentation and edge maps are produced by the two branches that make up the multi-tasking module via a convolutional layer with a kernel size of 11 and a deconvolutional layer, respectively (Zhihong et al., 2018). The multi-scale segmentation maps and multi-scale edge maps are the outputs of this network. The multitask network loss function is defined as

$$L_{multi-net} = -\sum_{k=1}^{k}\left\{\frac{1}{M}\sum_{j=1}^{M}\sum_{s=1}^{s}\sigma(l_j = s)\,log\,P_{j,s}^{s_k} + (fi = C)\,log\,p_{j,s}^{F_k}\right\}$$

Where the scales, picture pixels, and classes are denoted by the letters K, M, and S. Edge segmentation's and segmentation's ground truth maps are l and F. Segmentation and edge's ground truth map is represented by l and F. The actual labels for points j are lj and fj. P_(j,s)^(s_k) refers to the output likelihood that pixel j belongs to a particular segmentation map class. P_(j,s)^(F_k) represents the likelihood that pixel i belongs to the Cth class of the kth edge map. C = 1, 2 on the segmentation map stands for cancer and non-cancer cells, respectively. The backdrop and edge of the cancer cells are represented by the values C=1, 2 in the edge map, respectively. An indicator function () returns 1 when lj or fi are equal to 1 or 0 otherwise.

2.1.2. Global Network

The field is still rather small compared to the actual image, making it unable to capture the overall context, even though the dilated convolution layers expand the receptive area to prevent loss of image data. By selecting various areas of the image, the data obtained from these areas is combined to obtain more information about the overall context of the real receptive area of the CNN. GlobalNet performs this function. The output of the final block from the Multitasknet serves as the input to GlobalNet, as depicted in the picture. 4 deconvolutional layers and 5 convolutional layers are present. The 1x1, 2x2, and 3x3 subregional scales are used as alternatives. Following average pooling, the dimension is reduced using a convolutional layer with an 11 kernel before upsampling with bilinear interpolation to match the size of the input feature maps. To focus more on the global information, the depth of the input feature maps is lowered to 32 using a convolutional layer with a 3x3 kernel and then mixed with the upsampling results of different size sub-regions. Then, a deconvolution layer, a third layer, and two convolutional layers with kernels of 3x3 and 1x1 are used to create the segmentation result for a global context. Prediction models are employed that are described by the softmax loss function.

$$L_{Global} = \frac{-1}{M}\sum_{j=1}^{m}\sum_{s=1}^{s}\sigma(l_i = s)\,log\,P_{j,s}^{G}$$

Where P^G is the segmentation map generated by the output probability that pixel i belongs to a particular class.

2.1.3. Fusion Network

The FusionNet learns from the segmentation results obtained from Multitasknet and Globalnet which is further used to classify the cancer cells to stage 1, stage 2, or normal. The model is made up of five convolutional blocks, the first two of which consist of two convolutional layers that turn all of the pixels in the receptive field into a single value. It is followed by a stride 2 max-pooling layer of kernel size 2x2 that computes the maximum value for each feature map patch. Three convolutional layers are followed by a Max Pooling layer with a kernel size of 2x2 and stride 2 in the other three blocks. The network's result is the classification model file.

3. Execution environment and evaluation metrics

3.1. Network configuration

The network is built using the TensorFlow framework with high-level deep learning API Keras. The patch-based network is executed in GPUs (128GB RAM). The learning rate is initially set to 0.001. To train, the Adam optimizer is employed with a batch size of 32 and a total of 50 epochs.

3.2. Evaluation metrics

These performance metrics – Intersection over union, accuracy, precision, recall, and F-score – have been used to evaluate the segmentation and classification accuracy.

Intersection over union is a metric that indicates the degree of overlap between the segmentation region and the ground truth. If there are N number of overall classes indexed from {1…N}. Let C be a NxN confusion matrix of the selected classification method, where each item C_{ii} representing several samples from the class j predicted by the ground truth I.

The IoU per class I is defined as

$$IoU = Area\ of\ Overlap\ /\ Area\ of\ Union$$

Class I's evaluation metric is given as

$$IOU = C_{ii} / C_{ii} + \sum_{j \neq i} C_{ii} + \sum k \neq i$$

Accuracy describes the model's performance across all classes. It is determined as the ratio of correct predictions to total predictions.

$$Accuracy = \frac{TP + TN}{TP + FP + TN + FN}$$

Precision is defined as the ratio of true positives to all positives.

$$Precision = \frac{TP}{TP + FP}$$

Recall is calculated as the percentage of Positive samples that were accurately labeled as Positive samples relative to all Positive samples.

$$Recall = \frac{TP}{TP + FN}$$

F-Score is a metric that is used to assess the performance of a model. The goal of F-Score is to balance precision with recall, which is especially important when the positive class is infrequent.

$$F - score = \frac{2 \times (Precision \times Recall)}{Precision + Recall}$$

3.3. Models and technique used

MIFNET is compared with U-Net and V-Net for both segmentation and classification accuracy.

3.3.1. U-Net

The U-Net model's architecture is u-shaped. Both a contracting path and an expansive path are present. In the contracting path, the rectified linear units (ReLU) and maximum pooling techniques are performed after each iteration of the standard convolutional networks. While minimizing spatial information, the contraction enhances feature information. The expanding pathway unifies the

feature and spatial data via a succession of up-convolutions and concatenations with high-resolution features from the contracting path (Teramoto et al., 2021).

3.3.2. V-Net

It is a fully connected network-based model used in the segmentation of medical images. The data is decompressed until it reaches its original size on the right part of the V-Net design, which has compression paths on the left. The convolution layers employ volumetric kernels, and each stage involves the learning of a residual function. To provide two-channel probabilistic segmentation for both foreground and background regions, the decompression network pulls features from low-resolution feature maps and enhances their spatial representation (Milletari et al., 2016).

3.3.3. Transfer Learning

Transfer learning is a technique for applying knowledge from a previously trained model to new tasks. Problems involving classification, regression, and clustering can be solved via transfer learning. To classify images, the study makes use of the pre-trained model VGG-16 with Deep Convolutional Neural Network (Tammina et al., 2019). The convolution neural network (CNN) model VGG16, also known as VGGNet, supports 16 layers. Because VGG has a smaller convolutional filter, the network's propensity to over-fit during training sessions is reduced.

In this case, the outputs of MIFNET are given to the Fusionnet layer and replaced with VGG16 for classification. A transfer learning approach is used for classification, which uses pre-trained weights from VGG16 and the final output layer is modified with three fully connected layers & softmax to classify the output in one of the three cases – normal, stage 1, and stage 2., The classification accuracy of MIFNET is analyzed in comparison with the V-Net and U-Net. The segmentation accuracy directly impacts the classification accuracy of the models. Poor segmentation results in incorrect classification.

3.4. Performance evaluation

The performance of the MIFNET is assessed individually and concerning other networks such as U-NET and V-NET.

3.4.1. MIFNET Performance

The performance of the MIFNET in terms of accuracy and loss is shown in Figure 3-6 below. The Figure 3 shows that the MIFNET algorithm achieved a maximum accuracy of 99% for 50 epochs.

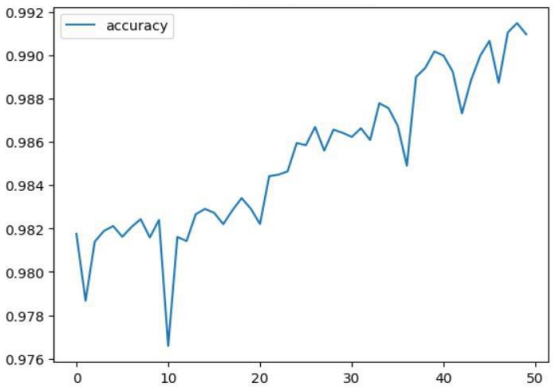

Figure 3. Training Accuracy

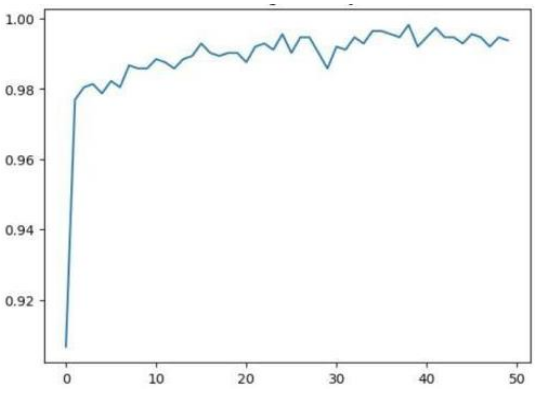

Figure 4. Testing Accuracy

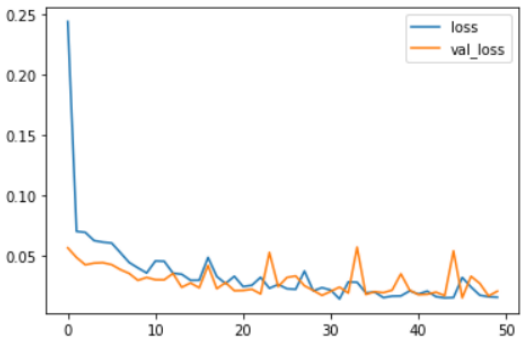

Figure 5. Accuracy vs Epoch

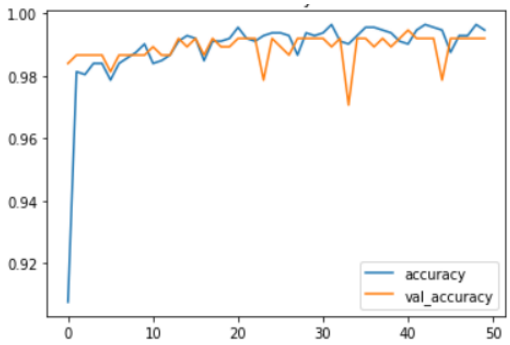

Figure 6. Loss Vs Epoch

4. Comparison with other models

Hyperparameters are set for MIFNET, U-NET, and V-NET with Adam as an optimizer, the batch size is 32, the number of epochs is 50, the learning rate is 0.001 and the execution environment is GPU (128GB RAM) in Ubuntu 20.01 OS.

4.1. Segmentation results

The Segmentation accuracy for the models is shown in Table 1. The results show that MIFNET produces better segmentation accuracy in segmenting the stage 1 and stage 2 cancer cells with an overall accuracy of 87%. The model segments the cancerous region only if it is present in the image.

Table 1. Segmentation Accuracy of MIFNET, U-Net, and V-Net

STAGE	MIFNET	U-NET	V-NET
Stage 1	92	75	68
Stage2	85	69	63
Accuracy	87	72	65

Further, results from Table 1 show that the segmentation accuracy for stage 1 and stage 2 is comparatively low producing 75% for U-Net and 69% for V-Net. Similarly, for stage 2 U-Net and V-Net produced 68% and 63% respectively. The reason for the low accuracy is due to insufficient edge information and global context, the edge precision and segmentation of cancer cells are lower and coarser causing it unable to detect the cancerous region precisely. However, the MIFNET model can learn the edge information and global context resulting in improved segmentation accuracy of cancer regions from the histopathological images.

4.2. Classification results

MIFNET modified with a classification layer is compared with V-Net and U-Net added with a classification layer. Then the classification accuracy for various metrics in terms of precision, recall, and f-score is computed and it is shown in Table 2. From the table it is seen that MIFNET has a higher precision value, implying that the model's positive predictions turn out to be accurate. Also, the MIFNET model shows a superior F1-Score than U-Net and V-Net, proving that its result is more precise and has a higher recall value i.e., a higher number of correct positive predictions out of all the positive predictions that could have been made.

Table 2. Classification Performance Report of Mifnet, Unet & Vnet

	MIFNET			**U-NET +VGG16**			**V-NET +VGG16**		
	Precision	Recall	F-Score	Precision	Recall	F-Score	Precision	Recall	F-score
Normal	100	100	100	100	100	100	100	100	100
Stage1	98	100	99	83	100	91	99	75	85
Stage2	100	98	99	100	81	89	81	99	89
Accuracy	99			93			91		

The visual outputs for all the cases for the 3 models are shown for two instances from Figure 7 to Figure 9. Figure 7 shows the normal cases detected by MIFNET, U-Net, and V-net. The top figures show the histopathological outputs and the bottom one shows the corresponding detection results by the 3 models. It is seen that no anomaly is detected for all the models showing 100% accuracy. Figure 8 shows the stage 1 detection. The dark pink circle represents the cancer cells, it can be seen that MIFNET can detect the cancer cells but the other 2 models are not. Similarly, the dark pink regions in Figure 9 show the cancerous region of stage 2. In this case, MIFNET can precisely detect the cancerous region while the other 2 models detect even the normal region as a cancer-infected region.

Results show that all three models can classify normal cases correctly. However, due to the presence of skip connections, which enforce a tight fusion approach and cause the encoder and decoder networks to accumulate the same scale feature maps, both U-Net and V-Net are not able to segment the stage-1 cancer cells, therefore classifying them as normal (as shown in Figure 8). In terms of stage-2 cancer, MIFNET performs better segmentation of the malignant region when compared to the other two models, thus giving a better picture of the region that is considered as stage-2 cancer (as shown in Figure 9).

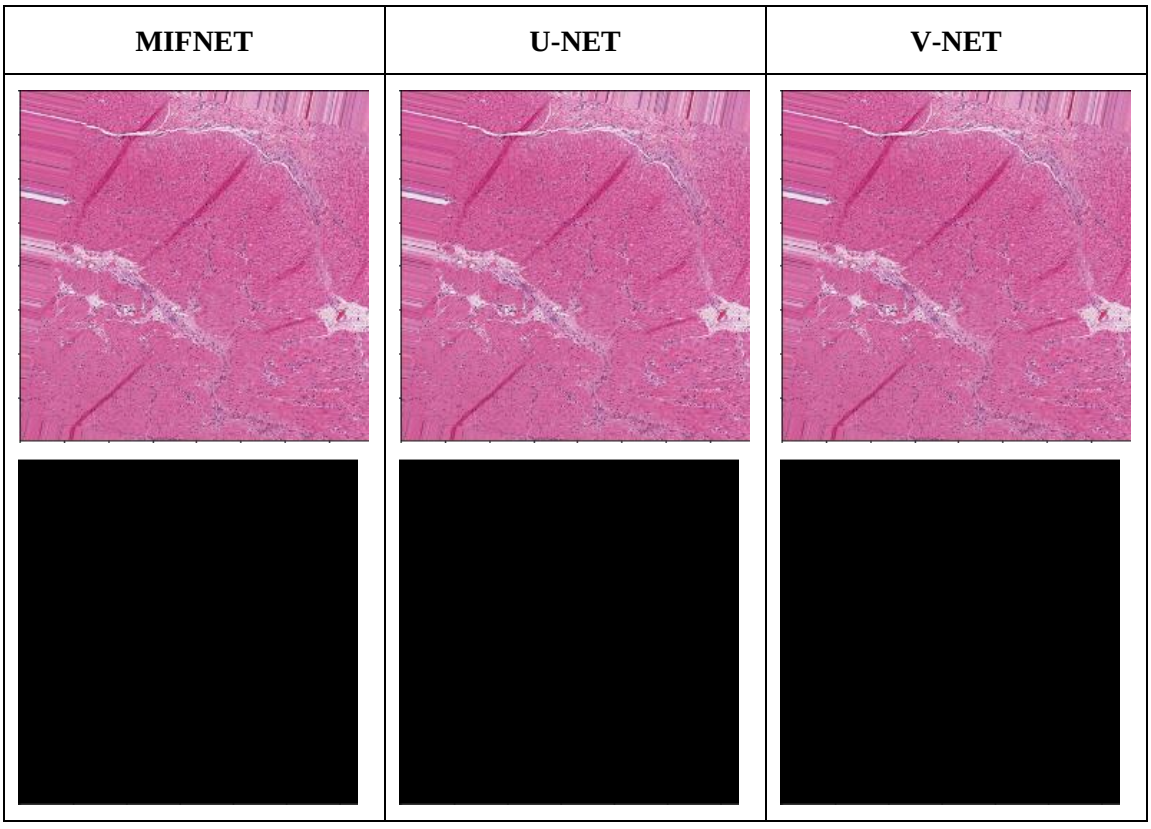

Figure 7. Case Norma

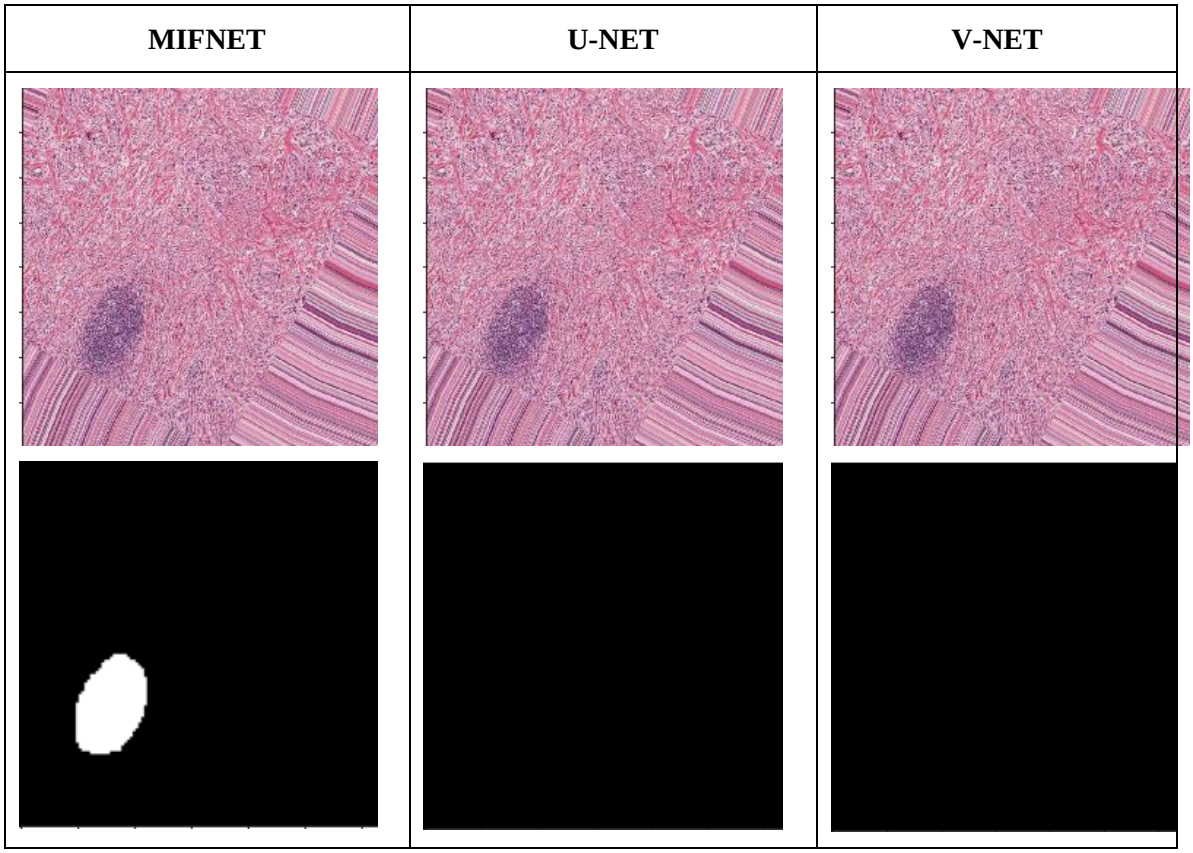

Figure 8. Stage-1 gastric cancer

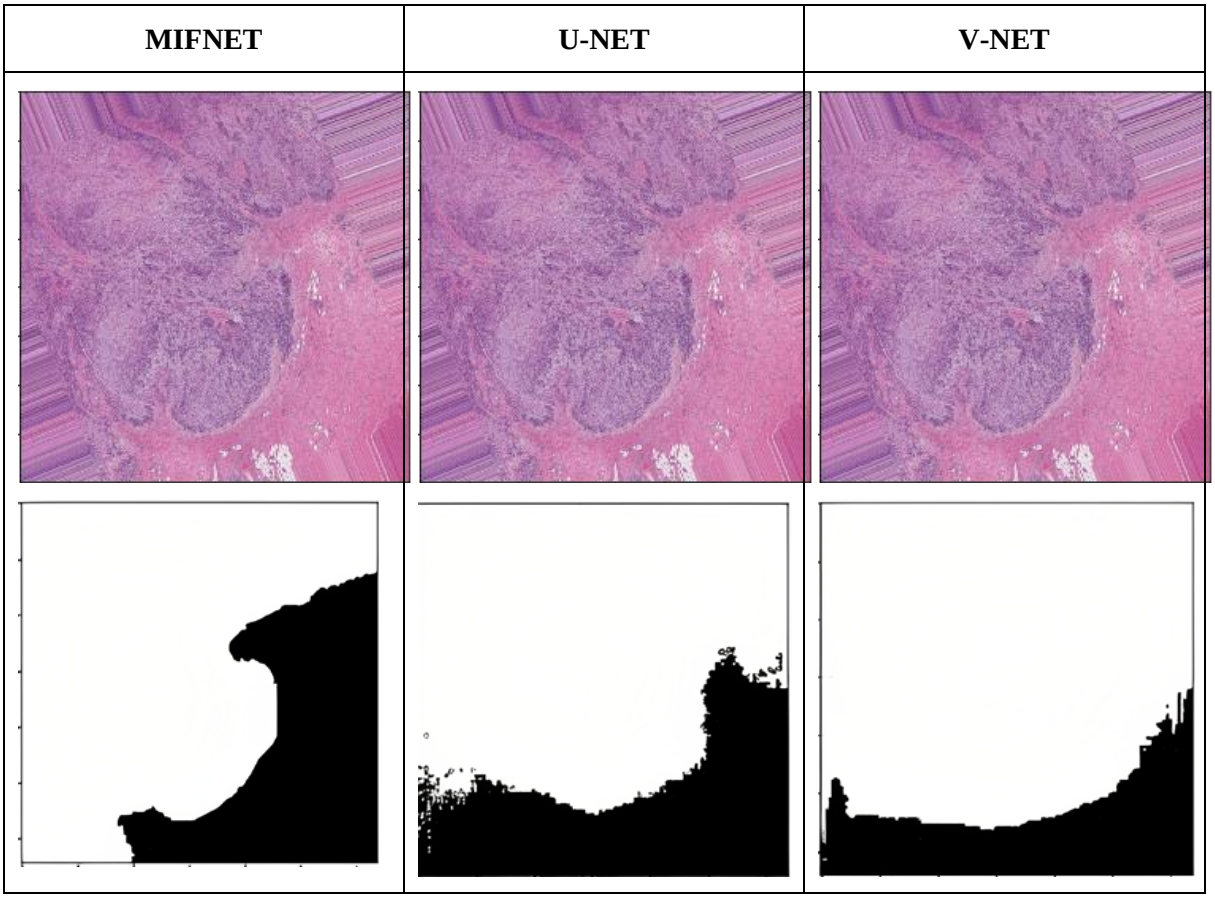

Figure 9. Stage-2 gastric cancer

5. Conclusion and future directions

In this study, a multi-information fusion paradigm for the detection and classification of gastric cancer is provided. To obtain more accurate segmentation and finer edges from the histopathology images, a network that trains to fuse multiple scales and sources is constructed. Compared with U-Net and V-Net, the proposed model improves the segmentation results of detecting irregular gastric cancer cells. Also, visualization and classification features were added to existing MIFNET to aid the clinician in diagnosing gastric cancer. Further, incorporating a classification model to MIFNET results in better classification accuracy compared to its other counterparts as well.

In the future, the aim is to increase the segmentation accuracy for better localization of the malignant cells by modifying the MIFNET architecture to gain more information about the input images, thus improving the detection accuracy of the cancer cells. Also, time series analysis for the progression of stomach cancer is another direction of improvement.

REFERENCES

Bray, F., Ferlay, J., Soerjomataram, I., Siegel, R. L., Torre, L. A. & Jemal, A. (2018) Global cancer statistics 2018: GLOBOCAN estimates of incidence and mortality worldwide for 36 cancers in 185 countries. *CA: A Cancer Journal for Clinicians*. 68(6), 394–424. doi: 10.3322/caac.21492.

Doyama, H., Yoshida, N., Tsuyama, S., Ota, R., Takeda, Y., Nakanishi, H., Tsuji, K., Tominaga, K., Tsuji, S., Takemura, K., Yamada, S., Katayanagi, K., Kurumaya, H., Iwashita, A. & Yao, K. (2015) The "white globe appearance" (WGA): a novel marker for a correct diagnosis of early gastric cancer by magnifying endoscopy with narrow-band imaging (M-NBI). *Endoscopy International Open*. 3(2), E120–E124. doi: 10.1055/s-0034-1391026.

Duffy, M. J., Lamerz, R., Haglund, C., Nicolini, A., Kalousová, M., Holubec, L. & Sturgeon, C. (2014). Tumor markers in colorectal cancer, gastric cancer, and gastrointestinal stromal cancers: European group on tumor markers 2014 guidelines update. *International Journal of Cancer*. 134(11), 2513–2522. doi: 10.1002/ijc.28384.

Hirasawa, T., Aoyama, K., Tanimoto, T., Ishihara, S., Shichijo, S., Ozawa, T., Ohnishi, T., Fujishiro, M., Matsuo, K., Fujisaki, J. & Tada, T. (2018) Application of artificial intelligence using a convolutional neural network for detecting gastric cancer in endoscopic images. *Gastric cancer: Official Journal of the International Gastric Cancer Association and the Japanese Gastric Cancer Association*. 21(4), 653–660. doi: 10.1007/s10120-018-0793-2

Huneburg, R., Marwitz, T., van Heteren, P., Weismüller, T. J., Trebicka, J., Adam, R., Aretz, S., Perez Bouza, A., Pantelis, D., Kalff, J. C., Nattermann, J. & Strassburg, C. P. (2016) Chromoendoscopy in combination with random biopsies does not improve detection of gastric cancer foci in CDH1 mutation-positive patients. *Endoscopy International Open*. 4(12), E1305–E1310. doi: 10.1055/s-0042-112582.

Ishihara, K., Ogawa, T. & Haseyama, M. (2017) Detection of gastric cancer risk from X-ray images via patch-based convolutional neural network. In: 2017 *IEEE International Conference on Image Processing (ICIP), 17-20 September, 2017, Beijing, China*. pp. 2055-2059. doi: 10.1109/ICIP.2017.8296643.

Katai, H., Ishikawa, T., Akazawa, K., Isobe, Y., Miyashiro, I., Oda, I., Tsujitani, S., Ono, H., Tanabe, S., Fukagawa, T., Nunobe, S., Kakeji, Y., Nashimoto, A. & Registration Committee of the Japanese Gastric Cancer Association (2018) Five-year survival analysis of surgically resected gastric cancer cases in Japan: a retrospective analysis of more than 100,000 patients from the nationwide registry of the Japanese Gastric Cancer Association (2001-2007). *Gastric cancer: Official Journal of the International Gastric Cancer Association and the Japanese Gastric Cancer Association*. 21(1), 144–154. doi: 10.1007/s10120-017-0716-7.

Li, Y., Deng, L., Yang, X., Liu, Z., Zhao, X., Huang, F., Zhu, S., Chen, X., Chen, Z. & Zhang, W. (2019) Early diagnosis of gastric cancer based on deep learning combined with the spectral-spatial classification method. *Biomedical Optics Express*. 10(10), 4999-5014. doi: 10.1364/BOE.10.004999.

Li, Y., Li, X., Xie, X. & Shen, L. (2018) Deep learning based gastric cancer identification. In: *2018 IEEE 15th International Symposium on Biomedical Imaging (ISBI 2018), 04-07 April, 2018, Washington, DC, USA*. pp. 182-185. doi: 10.1109/ISBI.2018.8363550.

Li, Y., Wu, Y., Huang, M., Zhang, Y., Bai, Z. (2023) Attention-guided multi-scale learning network for automatic prostate and tumor segmentation on MRI. *Computers in Biology and Medicine*. 165, 107374. doi: 10.1016/j.compbiomed.2023.107374.

Miller, K. D., Siegel, R. L., Lin, C. C., Mariotto, A. B., Kramer, J. L., Rowland, J. H., Stein, K. D., Alteri, R. & Jemal, A. (2016) Cancer treatment and survivorship statistics, 2016. *CA: A Cancer Journal for Clinicians*. 66(4), 271–289. doi: 10.3322/caac.21349.

Milletari, F., Navab, N. & Ahmadi, S. (2016). V-Net: Fully Convolutional Neural Networks for Volumetric Medical Image Segmentation. In: *2016 Fourth International Conference on 3D Vision, 25-28 October, 2016, Stanford, CA, USA.* pp. 565-571. doi: 10.1109/3DV.2016.79.

Sakai, Y., Takemoto, S., Hori, K., Nishimura, M., Ikematsu, H., Yano, T. & Yokota, H. (2018) Automatic detection of early gastric cancer in endoscopic images using a transferring convolutional neural network. In: *2018 40th Annual International Conference of the IEEE Engineering in Medicine and Biology Society (EMBC), 18-21 July, 2018, Honolulu, HI, USA.* pp. 4138–4141. doi: 10.1109/EMBC.2018.8513274.

Siegel, R. L., Miller, K. D. & Jemal, A. (2023) Cancer statistics, 2023. *CA: A Cancer Journal for Clinicians*. 73(1), 7-30. doi:10.3322/caac.1840.

Tammina, S. (2019) Transfer learning using VGG-16 with Deep Convolutional Neural Network for Classifying Images. *International Journal of Scientific and Research Publications*. 9(10), 9420. doi: 10.29322/IJSRP.9.10.2019.p9420.

Teramoto, A., Shibata, T., Yamada, H., Hirooka, Y., Saito, K., Fujita, H. (2021) Automated Detection of Gastric Cancer by Retrospective Endoscopic Image Dataset Using U-Net R-CNN. *Applied Sciences*. 11(23), 11275. doi: 10.3390/app11231127.

van der Post, R. S., van Dieren, J., Grelack, A., Hoogerbrugge, N., van der Kolk, L. E., Snaebjornsson, P., Lansdorp-Vogelaar, I., van Krieken, J. H., Bisseling, T. M. & Cats, A. (2018) Outcomes of screening gastroscopy in first-degree relatives of patients fulfilling hereditary diffuse gastric cancer criteria. *Gastrointestinal Endoscopy*. 87(2), 397–404. doi: 10.1016/j.gie.2017.04.016.

Wang, T. (2021) *SEED-gastric carcinoma dataset*. https://www.kaggle.com/datasets/wangtyi/seedgastric-carcinoma-dataset [Accessed 28th October 2023].

Zhang, J., Li, G. & Jiang, S. (2022) Survival outcomes of patients with stomach cancer in the United States: A population-based study. Cancer Epidemiology. *Biomarkers & Prevention*. 31(3), 623-630. doi:10.1158/1055-9965.EPI-22-0076.

Zhihong, P., Hao, D., Jiaxing, M., Min, D. & Jinwen, T. (2018) MIFNet: Multi-Information Fusion Network for Sea-Land Segmentation. In: *ICAIP '18: Proceedings of the 2nd International Conference on Advances in Image Processing, 16-18 June, 2018, Chengdu, China.* pp. 24–29. doi: 10.1145/3239576.3239578.

Varghese Sicily Felix ENIGO received her Ph.D. Degree in Computer Science and Engineering from Anna University from Chennai India in 2015. Her area of research includes Artificial Intelligence, Internet of Things, and Internet Technologies. Dr. Felix Enigo is currently an Associate Professor at the Department of Computer Science & Engineering, SSN College of Engineering, Chennai, Tamil Nadu, India. She was one of the recipients of the BIG-16 award by BIRAC, Department of BioTechnology, Government of India. She has worked on various industry-based consultancy projects and funded projects.

Rajashree SHANMUGANATHAN obtained her Bachelor's degree in Computer Science and Engineering from SSN College of Engineering. She is currently working as a software engineer. Her research interests include AI, Cloud computing, Deep Learning, and Machine Learning.

Sneha VENKATAPATHY graduated from SSN College of Engineering, with a Bachelor's degree in Computer Science and Engineering. She is currently a master's student. Her areas of interest include Data Analytics, Business, Internet of things and Deep learning,

Sahir RAHAMAN graduated from SSN College of Engineering, with a Bachelor's degree in Computer Science and Engineering. He is currently a software analyst. His research interests include Business, Cybersecurity, AI, and Deep Learning.